Characterization of pore structures of hydrated cements and natural shales by ^{129}Xe NMR spectroscopy

Bing Zhou[a], Sanna Komulainen[b], Juha Vaara[b], Ville-Veikko Telkki[b*]

[a] *School of Materials Science and Engineering, Tongji University, Shanghai 210000, China*

[b] *NMR Research Unit, University of Oulu, P.O.Box 3000, FIN-90014 University of Oulu, Finland*

** Corresponding author: E-mail address: ville-veikko.telkki@oulu.fi (V.-V. Telkki)*

ABSTRACT

^{129}Xe NMR of adsorbed xenon gas is a sensitive tool for the characterization of porous materials. Here we exploit, for the first time, ^{129}Xe NMR to investigate the nanoscale porous structures in hydrated white cements and natural shale. Signals of xenon in mesopores and larger voids are well resolved in the spectra of the cement samples, and the exchange rate between these sites was determined to be 100−300 s^{-1} at room temperature. The spectra imply that the mesopore size is the smallest and the exchange rate is the highest in the sample with the lowest initial water/cement ratio. The heat of adsorption of xenon in the cements is similar to that in silica gels, about 12 kJ/mol. The shale spectra include a very broad signal, covering a range of about 600 ppm, implying that the adsorbed xenon interacts with the paramagnetic impurities present in the samples.

Keywords:

^{129}Xe NMR spectroscopy

Cement

Shale

Porous material

1. Introduction

Cement is a binder used in the production of mortar and concrete [1]. The shale gas methane is becoming an increasingly important, unconventional source of energy in the world [2,3,4,5]. One of the most important characteristics of both cement and shale is the pore structure of the material. Pores have a dominating effect on the strength of cement, and they influence the transport properties, permeability and durability. In the case of gas shale, the micro- and mesoporous structure not only facilitates the adsorption and preservation of the gases, but also poses significant difficulties in the gas extraction. Therefore, it is very important to be able to characterize the pore structures of these materials.

Standard methods such as mercury intrusion porosimetry (MIP), microscopic techniques (TEM, SEM and FESEM), as well as small-angle X-ray and neutron scattering (SAXS and SANS), are very useful in the characterization of porous media, but they have also some limitations and they may be invasive and perturbing [6]. For example, in the MIP technique, requires the high pressures applied for (toxic) mercury invasion may perturb and damage the pore structure of the sample. The technique measures the size of the pore throat (entrance or interconnection regions between the pores), instead of the true volume within the pore. Obtaining high (below one nanometer) resolution with TEM or FESEM requires cutting the sample into slices with a thickness of only a few nanometers, which is very challenging. Without this kind of cutting, the resolution remains limited to typically >500 nm features, and the images do not provide information about micro- and mesopores.

Nuclear magnetic resonance (NMR) spectroscopy is a sensitive, noninvasive tool to probe the local physicochemical environments and dynamical processes at the atomic and molecular level [7]. It has also been applied to investigate the local structural features of minerals and the geochemical processes [8,9,10]. Diffusion, relaxation, NMR cryoporometry (NMRC) and magnetic resonance imaging (MRI) measurements of fluids adsorbed in porous materials provide detailed information

about the pore size distribution, morphology, transport and adsorption phenomena, as well as chemical exchange [11,12,13,14,15,16,17]. NMR relaxometry has been exploited to characterize porous structures of cements and shale [18,19,20,21,22,23,24,25,26,27,28,29,30,31,32,33]. Variable-temperature MRI of freezing water was also successfully employed to observe the spatially resolved pore size distribution in cements [34]. Pipilikaki and Beazi-Katsioti [35] investigated the porous structure in blended cements with different proportions of limestone, by means of MIP and NMR cryoporometry. Heterogeneity and paramagnetic iron oxide impurities of cement and shale samples lead to a rapid decay of the NMR signal and can render NMR analysis challenging. For example in Ref. [36], relaxation time distributions of various shale samples appeared to be independent of the sample and, hence, did not reflect the pore size distribution. Furthermore, NMRC measurements of mesopore sizes in cement and shale samples have turned out to be challenging [36].

Xenon is an inert, monoatomic gas having a van der Waals diameter of 4.3 Å. Xenon has two NMR-active isotopes, spin-1/2 ^{129}Xe and spin-3/2 ^{131}Xe. Xenon possesses an easily polarizable electron cloud, which renders the chemical shift of ^{129}Xe to be highly sensitive to its local environment [37,38]. The NMR sensitivity of ^{129}Xe can be increased by several orders of magnitude via spin-exchange optical pumping [39]. Therefore, ^{129}Xe NMR has been used as an inert probe, *e.g.*, in the MRI of lungs [40,41], microfluidic flow imaging [42,43], investigation of liquid crystals [44,45], polymers [46,47], and cages [48], as well as biosensor applications [49].

^{129}Xe NMR has turned out to be especially useful in the characterization of porous media [50]. Chemical shift of xenon adsorbed in pores provides detailed information about the pore size and geometry, as well as surface interactions in a broad variety of microporous, nano-structured materials. ^{129}Xe NMR was initially applied to crystalline microporous oxides such as zeolites and clathrates [51,52]. Later, its application range was extended to amorphous mesoporous materials such as silica [53,54], alumina [55] and carbonaceous materials [56]. It has been demonstrated that the introduction of a liquid or solid medium into a mesoporous material slows down the inter-pore exchange of xenon,

which facilitates the determination of pore size distribution [57,58,59,60,61]. ^{129}Xe NMR spectroscopy has successfully been applied to investigate natural samples such as soil [62], clays and pillared clays [63], coals [56] and stones [64], and it is has also been exploited to determine the lattice boron content [65]. The experimentally determined correlations between the chemical shift and pore size [50,51,54,55,61] may be used for the characterization of unknown pore structures. Naturally, such correlations between ^{129}Xe NMR parameters and porous characteristics are complicated by many factors in samples such as pore heterogeneity, organic functional groups, the presence of paramagnetic compounds, occurrences of xenon exchange between inter- and intraparticle void spaces, texture and composition [50].

Here, we use ^{129}Xe NMR to characterize cement and shale samples. To the best of our knowledge, this the first time the method is applied to these materials. The two kinds of materials have similarities in their chemical and mineral composition, as well as texture, since both materials are basically silicates. On the other hand, shale materials are more heterogeneous and they include a larger concentration of paramagnetic impurities. The comparison of NMR results obtained from cement and shale samples can provide useful information about the similarities and differences of the two materials. We exploit the sensitivity of the ^{129}Xe chemical shift to estimate the sizes of mesopores in the materials, as well as to reveal the existence of paramagnetic sites. With variable-temperature experiments, we determine the heats of adsorption, and with two-dimensional exchange spectroscopy (EXSY) [66], we probe the dynamics of xenon atoms in the materials. The van der Waals diameter of xenon (4.3 Å) is close to the kinetic diameter of methane (3.8 Å) and, therefore, xenon is expected to probe structures in which also methane exists in shale.

2. Materials and Methods

2.1 Materials

Commercial anhydrous cement was purchased from BASF. Three samples were hydrated and prepared using an initial water/cement ratio of 0.1, 0.3 and 0.5; thus, the samples are referred to as C0.1, C0.3 and C0.5, respectively. After a 4-month hydration period, the cement samples were stored in closed containers at constant temperature (20 °C and 100% relative humidity). Before the NMR experiments, the samples were ground and sieved until most of the material passed through a 63 μm sieve.

The black shale core samples were collected from the Cambrian-Silurian strata at the Low Yangzi Plateau in China. This source is well known for the sedimentary facies with abundant organic materials, which are the most important exploration targets for shale gas in China. One of the shale samples under investigation was from Hubei Province of China, while two other samples were from Chongqing. Although belonging to the same strata, the distance between these two locations is over 500 km. The three shale samples were labeled as HU234, CH2175 and CH3634, where HU and CH refers to Hubei and Chongqing, respectively, and the number corresponds to the depth in meter, from which the sample was drilled. Before the NMR experiments, the shale samples were ground and sieved using the same procedure as the cement samples.

2.2 ^{129}Xe NMR experiments

Ground cement or shale samples were inserted in a 10 mm heavy-wall NMR tube, and dried overnight in an oven, in vacuum at the temperature of 70°C. Thereafter, a proper amount of ^{129}Xe isotope-enriched (91%) xenon gas was condensed into the NMR tube by immersing the tube in liquid N_2, and the tube was sealed with a flame. The xenon pressure in the tube was *ca.* 4 atm.

^{129}Xe NMR spectra were measured out using Bruker Avance III 300 spectrometer with the magnetic field of 7.1 T, ^{129}Xe frequency of 83 MHz and a 10-mm BBFO probe. Temperature series (from 225 to 300 K) were measured with a temperature stabilization time of 30 min with about

10 K steps. The reading temperatures were calibrated with standard Bruker samples. ^{129}Xe chemical shifts were referenced with respect to low-pressure Xe gas. The spectra were measured using the spin-echo pulse sequence. The lengths of the 90° and 180° pulses were 36 and 72 μs, and the delay τ before and after the 180° was 1 μs. The number of accumulated scans was 1026 and 4096, and the recycling delay was 1 and 0.5 s for the cement and shale samples, respectively.

Two-dimensional ^{129}Xe EXSY spectra of the cement samples were measured using Bruker Avance III 400 spectrometer at the magnetic field of 9.4 T, ^{129}Xe frequency of 110.7 MHz and a 10-mm BBFO probe. The length of the 90° pulse was 41.6 μs. The number of accumulated scans was 1024, the recycling delay was 0.5 s, and the mixing times τ_{mix} varied from 0.5 ms to 100 ms.

3. Results and Discussion

3.1 FESEM, EDS and XRD analysis

Field Emission Scanning Electron Microscope (FESEM) and Energy-Dispersive X-ray Spectroscopy (EDS) analysis showed that the texture of the cement samples is much more homogeneous than that of the shale samples. No paramagnetic impurities were detected in the cement samples. According to the X-ray diffraction (XRD) analysis, the shale samples were mainly composed of clay minerals such as kaolinite, illite, and montmorillonite, as well as ~10 wt % or more of very fine-grained quartz and feldspars. Calcite and dolomite were also detected in the XRD analysis. The content of paramagnetic Fe/Mn-bearing minerals such as pyrite [67] was below 4 wt %.

3.2 ^{129}Xe spin echo NMR spectra of the cement and shale samples at 290 K

^{129}Xe NMR spectra of xenon adsorbed in the cement and shale samples, measured in the standard way with a 90° excitation pulse followed by the detection of the free induction decay

(FID) signal at 7.1 T field, resulted in a distorted background of the spectrum. The problem was especially severe in the case of the shale samples due to their paramagnetic impurities, and it was difficult to resolve the true signals from the background distortion. The distortions were efficiently eliminated using a spin-echo experiment, in which the delay τ before and after the 90° refocusing pulse was 1 μs only due to the short T_2 of adsorbed ^{129}Xe. We validated that we do not mix true signals with background distortion by comparing the ^{129}Xe spectra of the shale samples with and without xenon.

^{129}Xe spin-echo NMR spectra of the hydrated cement samples measured at 290 K, are shown in Fig. 1a. The spectra include two signals: an intense signal at around 5 ppm chemical shift, arising from the xenon gas within the large material pores, as well as the interparticle space, called free gas signal, and another, weaker but broad signal around 30-50 ppm from xenon adsorbed in mesopores. The correlation between the chemical shift of ^{129}Xe and pore size determined using silica-based materials [54] implies that the size of these mesopores is between 10 and 50 nm, being in agreement with the pore size distributions obtained by N2 gas sorption measurements. The chemical shift of the mesopore signal of C0.1 is larger than that of the two other samples, which suggests that the size of mesopores is smaller in this sample than in the others. This may be a consequence of the low initial water/cement ratio of the C0.1 sample, which resulted in a lower degree of hydration and, consequently, smaller pores.

^{129}Xe spin-echo NMR spectra of the shale samples are shown in Fig. 1b. The spectra include an extremely broad signal, extending from about -300 to 300 ppm. Strictly speaking, the spectra shown in Fig. 1b are sums of two spin-echo experiments carried out with different carrier frequencies, which were at 0 and 200 ppm. The excitation range of the 180° pulse with a pulse length of 72 μs was only about 300 ppm, and therefore the full frequency range was not observed in a single experiment, but it required at least two experiments with two different carrier frequencies.

Experiments with a broader range of carrier frequencies (not shown) confirmed that the spectrum shown in Fig. 1b covers the entire signal range. Because the excitation ranges in these two experiments were partially overlapping and the excitation profiles were not constant over the whole signal region, the spectra are weighted by the overlapping and excitation profile. Regardless of these issues, the spectra provide qualitative representation of the ^{129}Xe chemical shift ranges in the samples.

Large negative chemical shifts in the ^{129}Xe spectral patterns of the shale samples have to be a consequence of the interactions of ^{129}Xe with paramagnetic Fe/Mn-bearing minerals, because the interactions with diamagnetic substances produce only positive or, at most, slightly negative shifts with respect to free, dilute xenon gas. This is due to the fact that the primary mechanism for the NMR chemical shift of chemically unbound, atomic xenon is via orbital paramagnetism inflicting a negative shielding and positive chemical shift contribution in diamagnetic compounds [68]. A tight confinement in small pores means that a significant density of virtual electronic states is available for the orbital paramagnetic chemical shift mechanism to operate through, explaining a large positive ^{129}Xe shift.

In electronically open-shell situations, such as in the presence of paramagnetic ions, both the contact and pseudocontact chemical shift contributions [69] may gain both positive and negative values, depending on the sign of the electron spin density at the NMR nucleus, as well as its relative location with respect to the paramagnetic ion. Hence, the presence of negative experimental ^{129}Xe chemical shift signals compellingly suggests the influence of paramagnetic ions, which most probably also have a dominant effect on the shape of the spectra, both at positive and negative chemical shift values. All the spectra include two maxima, one around +50 ppm and another around -140 ppm. A possible explanation for this is the presence of two different locations of the Xe guests, positioned at oppositely signed lobes of the isosurfaces of pseudocontact shifts, as dictated by the principal axis system of the magnetic susceptibility tensor of the paramagnetic impurity (see [69,70], and references therein).

The ^{129}Xe chemical shift range and spectral shape are quite similar for all the three shale samples. In the case of the HU234 sample, the positive half of the chemical shift pattern is slightly more weighted than in the two other samples. This may be caused by different balance of the different Xe sites with respect to the paramagnetic impurities in HU234, as compared to the other samples. We note that, similarly to the predominantly diamagnetic cement samples, ^{129}Xe adsorbed in mesopores may contribute the signal around +50 ppm as well, via the normal orbital mechanism [68] and even without the effect of paramagnetic centers. Furthermore, ^{129}Xe inside micropores with a pore size smaller than 2 nm may induce resonances even in the large positive shift range of 100-300 ppm [51,54].

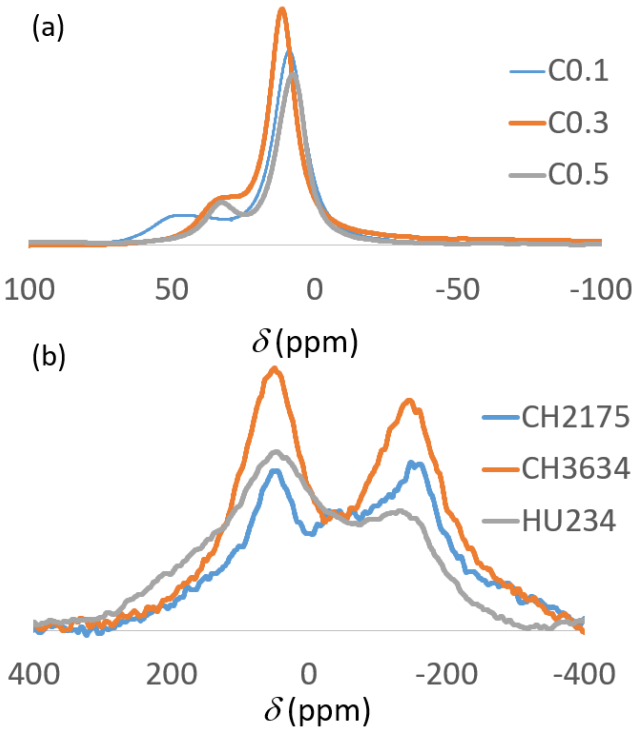

Fig. 1. ^{129}Xe spin echo spectra of (a) hydrated white cement and (b) shale samples measured at 7.1 T and 290 K.

3.3 Variable-temperature ^{129}Xe spin-echo NMR spectra of the cement and shale samples

^{129}Xe spectra of the cement samples measured at variable temperatures between 225 and 300 K are shown in Fig. 2. The chemical shift of the mesopore signal increases rapidly with decreasing temperature. Based on the assumption that the chemical shift δ(^{129}Xe) in mesoporous silica gels is a weighted average of the contributions of free and adsorbed Xe atoms, Terskikh *et al.* [53] derived the following empirical correlation:

$$\delta = \frac{\delta_S}{1+\frac{D}{\eta R\sqrt{T}K_0\exp(Q/RT)}}. \qquad (1)$$

Here, δ_S is the chemical shift of ^{129}Xe adsorbed on the surface of the pore, D is the mean pore size, η is the pore geometry factor (equal to 4 for cylindrical pores), R is the universal gas constant, T is the temperature, K_0 is the pre-exponential factor, and Q is the effective heat of adsorption. According to this model, the chemical shift increases with decreasing temperature, because the guest population in the adsorbed site increases.

Fits of Eq. 1 to the experimentally determined ^{129}Xe chemical shifts of the mesopore signals of the cement samples, are shown in Fig. 2d, and the resulting parameters are collected in Table 1. The heats of adsorption, about 12 kJ/mol, are the same for all the cement samples within the experimental error, and the value is within the range of the heats of adsorption determined for silica gels (8-21 kJ/mol [53]). The fitted chemical shift of ^{129}Xe adsorbed on the surface of the pore, about 240 ppm, is also independent on the sample within the experimental error. The value is much larger than those determined for silica, alumina and MCM-41 materials (116±3, 117±9 and 120±12 ppm, respectively) [54,55]. This may be a consequence of the different chemical structure of the pore surfaces as well as the very heterogeneous pore structure of the cement samples.

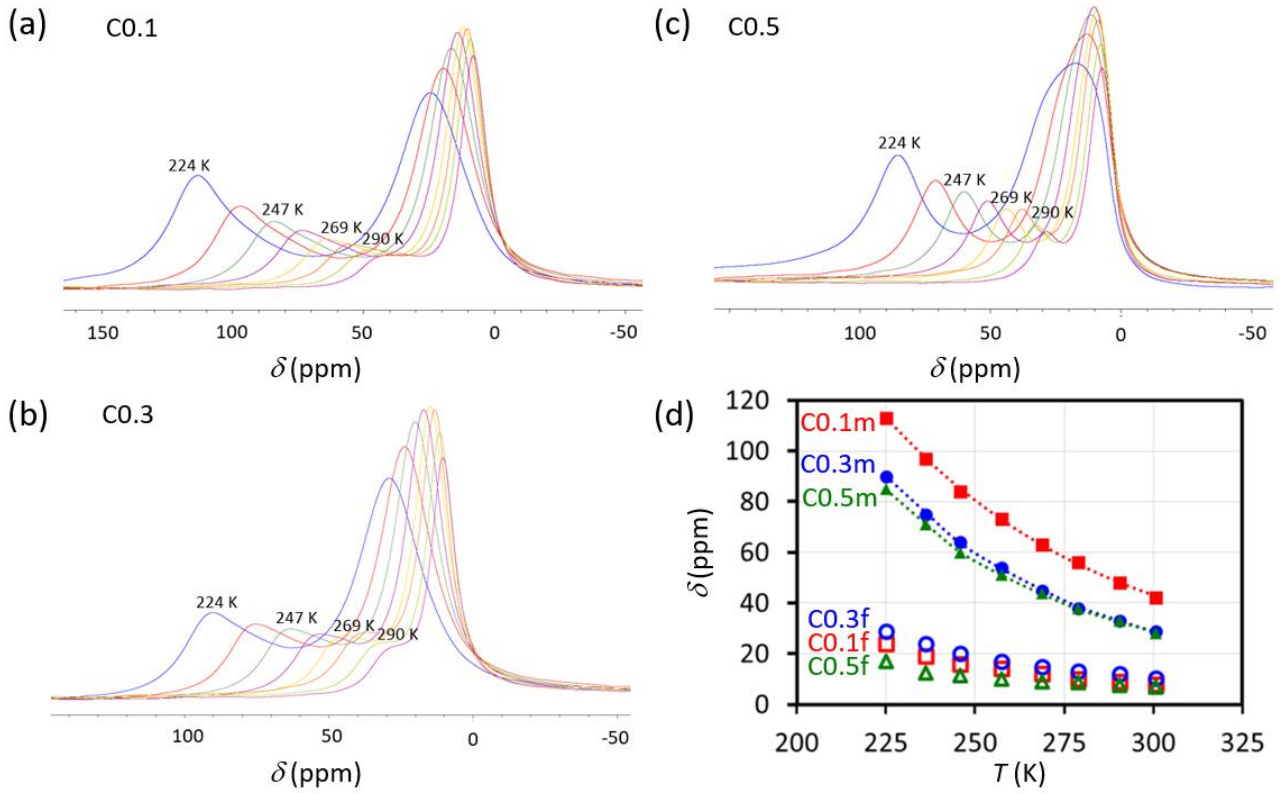

Fig. 2. Variable-temperature ^{129}Xe spin-echo NMR spectra of (a) C0.1, (b) C0.3, and (c) C0.5 cement samples. (d) Chemical shifts of the free gas (denoted by f) and mesopore (m) signals with temperature. Fits of Eq. 1 to the data points are shown by dashed lines.

Table 1

Parameters resulted from the fit of Eq. 1 to the experimental ^{129}Xe chemical shifts of the mesopore signals of the cement samples.

Sample	Q (kJ/mol)	δ_S (ppm)	$D/\eta K_0 R$ ($K^{1/2}$)
C0.1	11.5±0.6	240±30	11500±600
C0.3	12.5±0.5	210±20	16900±1500
C0.5	11.2±0.7	260±60	12200±900

Variable-temperature ^{129}Xe NMR spectra of the shale samples are shown in Fig. 3. Lowering the temperature from 290 to 230 K did not significantly change the shape and frequency range of the spectra. The positions of both the two maxima moved slightly toward higher chemical shifts (to the same direction, left in Fig. 3) with lowering temperature for all the shale samples, but the change was smaller than in the case of the mesopore signal of the cement samples. In the case of HU234, the amplitude of the smaller (negative) chemical shift maximum decreased significantly with lowering temperature, but the two other samples did not show similar behavior.

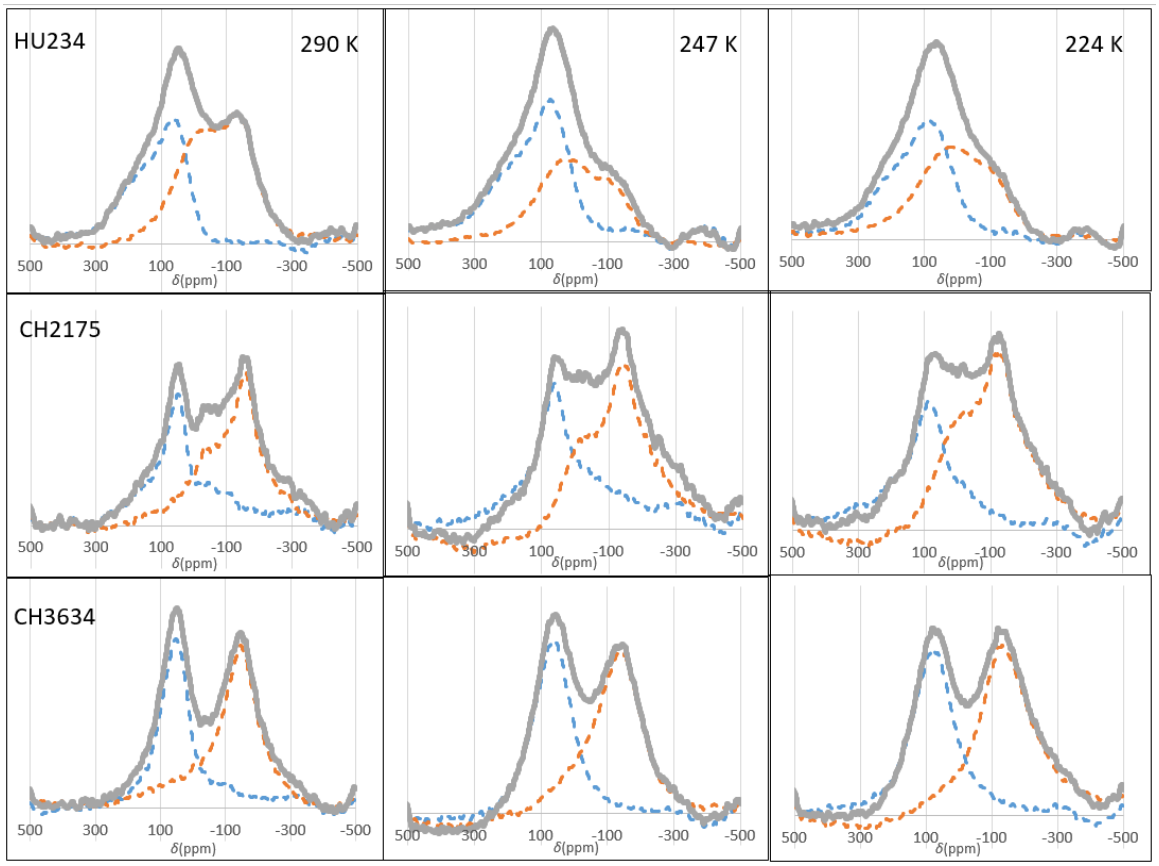

Fig. 3. Variable-temperature ^{129}Xe spin-echo NMR spectra of the shale samples. The overall spectra (gray solid lines) are sums of two subspectra measured at two different carrier frequencies, corresponding to 0 ppm (orange dashed line) and 200 ppm (blue dashed line).

3.4 ^{129}Xe EXSY of the cement samples

Two-dimensional ^{129}Xe EXSY spectra of the C0.1 cement sample measured at room temperature with varying mixing time τ_m, are shown in Fig. 4a. The cross peaks visible at longer mixing times indicate that exchange takes place between the free gas and mesopore sites. The fit of a two-site exchange model [66] to the amplitudes of the diagonal and cross peaks measured as a function of mixing time (see Fig 4b) resulted in the exchange rate *k* of 300±50 s^{-1} for C0.1, while the corresponding values for C0.3 and C0.5 are slightly lower, 70±30 and 100±30 s^{-1}, respectively (see Table 2). The chemical shifts of the mesopore signals imply that the size of pores are smaller in the C0.1 sample than in the other cement samples (see above). The exchange rates, in turn, suggest that these smaller mesopores in C0.1 have a better connection to the free gas site than the larger pores in the other cement samples. This may indicate that the mean distance between these sites is shorter in C0.1 than in the two other cement samples due to the lower degree of hydration.

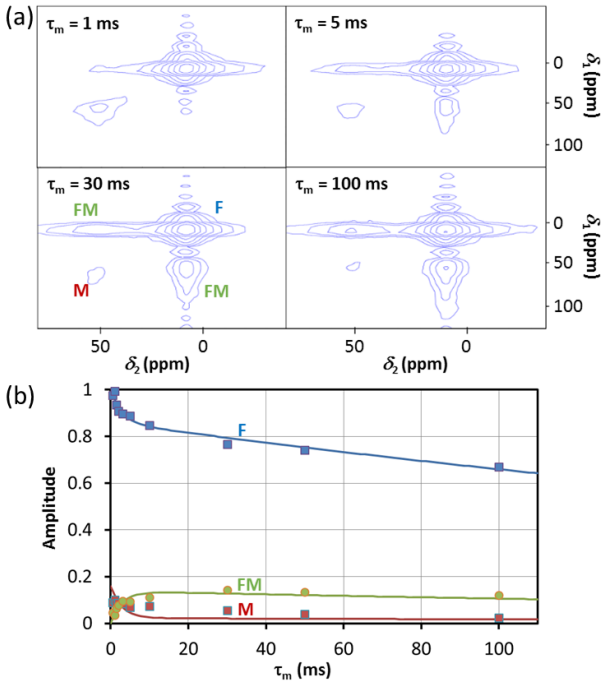

Fig. 4. (a) Two-dimensional ^{129}Xe EXSY spectra of the C0.1 cement sample measured at room temperature with variable mixing time τ_m shown in the figure. (b) Amplitudes of the diagonal free gas (F) and mesopore (M) signals, as well as the cross-peaks (FM) as a function of the mixing time, and a fit of the two-site exchange model to the experimental data (solid lines).

Table 2.

Parameters resulted from the fits of two-site exchange model to the amplitudes of EXSY signals of the cement samples. X_F and X_N are the relative populations of free gas and mesopore sites, respectively, k_{FN} is the exchange rate from the free gas site to the mesopore site, k_{NF} the other way around, and k is the overall exchange rate ($k = k_{FN} + k_{NF} = k_{FN}/X_N = k_{NF}/X_F$).

Sample	X_F	X_N	k_{FN} (s^{-1})	k_{NF} (s^{-1})	k (s^{-1})
C0.1	0.86±0.02	0.14±0.02	41±7	260±40	300±50
C0.3	0.81±0.03	0.19±0.03	13±5	50±20	70±30
C0.5	0.82±0.02	0.18±0.02	18±6	80±30	100±30

4. Conclusions

We have demonstrated, for the first time, that ^{129}Xe NMR of adsorbed xenon provides lots of important information about the pore and chemical structure as well as thermodynamics of cement and shale samples. The analysis implies that the size of the mesopores in the cement samples is between 10 and 50 nm, and the heat of adsorption is about 12 kJ/mol. Furthermore, chemical exchange takes place between the free gas and mesopore sites with the exchange rate of 100-300 s^{-1}, depending of the degree of hydration. Because the size of the Xe atom is similar to the size of methane, they are expected to probe similar environments in the shale samples. Very broad distribution of ^{129}Xe resonances is observed in the shale samples, featuring both positive and negative ^{129}Xe shifts, which implies that the adsorbed xenon interacts strongly with paramagnetic compounds. Paramagnetic compounds made the ^{129}Xe NMR experiment challenging, because they induced strong background signals and we were not able to excite the full spectral width with a single scan. However, spin-echo experiments efficiently removed the distortions, and the full spectral width was measured peace-wise by changing offset. The advantage of the paramagnetic interactions is that they magnify the chemical shift caused by the interactions between xenon and adsorption sites. Hence, the sensitivity of the chemical analysis is improved. Consequently, ^{129}Xe NMR has turned out to be a useful tool in the characterization of cement and shale materials of utmost importance in modern society. In the future, combination of the experimental method and state-of-the-art modeling of paramagnetic effects on the NMR parameters [71] is expected to provide detailed insight into the surface chemistry of such materials.

Acknowledgements

B.Z. acknowledges financial support from an NSFC Grant No. 41572103. V.-V.T. and J.V. acknowledge the Academy of Finland for financial support (grant numbers 289649, 294027 and

296292). We are thankful to Drs. Wu Yao and Dan Jin for providing white cement samples. The authors are grateful to Drs. Susanna Ahola and Anu Kantola for inspiring discussions and helping in the experimental issues. Furthermore, we thank Sami Hiltunen and Arttu Mankinen for helping in the sample preparation.

References

[1] P.-C. Aïtcin, Cem. Concr. Res. 30 (2000) 1349−1359.

[2] D.J.K. Ross, R.M. Bustin, Mar. Pet. Geol. 26 (2009) 916−927.

[3] E. Fathi, I.Y. Akkutlu, Transp. Por. Med. 80 (2009) 281−304.

[4] E. Fathi, I.Y. Akkutlu, Transp. Por. Med. 91 (2012) 5−33.

[5] M. Josh, L. Esteban, L. Delle, C. Piane, J. Sarout, D.N. Dewhurst, M.B.J. Clennell, Pet. Sci. Eng. 88-89 (2012) 107-124.

[6] F. Rouquerol, J. Rouquerol, K. Sing, Adsorption by powders and porous solids, Academic Press, San Diego, 1999.

[7] P.T. Callaghan, Translational dynamics and Magnetic Resonance: principles of Pulsed Gradient Spin Echo NMR, Oxford University Press, Oxford, USA, 2011.

[8] R. Kirkpatrick, B. Phillips, Appl. Magn. Reson. 4 (1993) 213-236.

[9] B.L. Sherriff, H. Grundy, J.S. Hartman, Eur. J. Mineral. 3 (1991**)** 751-768.

[10] B. Zhou, B.L. Sherriff, J.S. Hartman, G. Wu, Am. Mineral. 92 (2007) 34-43.

[11] J. Kärger, R. Valiullin, Chem. Soc. Rev. 42 (2013) 4172-4197.

[12] Y.-Q. Song, J. Magn. Reson. 229 (2013) 12-24.

[13] I.V. Koptyug, Prog. Nucl. Magn. Reson. Spectrosc. 65 (2012) 1-65.

[14] O.V. Petrov, I. Furó, Prog. Nucl. Magn. Reson. Spectrosc. 54 (2009) 97-122.

[15] J. Mitchell, J.B.W. Webber, J.H. Strange, Phys. Rep. 461 (2008) 1-36.

[16] S.D. Beyea, S.L. Codd, D.O. Kuethe, E. Fukushima, Magn. Reson. Imaging 21 (2003) 201-205.

[17] P.M. Kekkonen, A. Ylisassi, V.-V. Telkki, J. Phys. Chem. C118 (2014) 2146-2153.

[18] J.-P. Korb, L. Monteilheta, P.J. McDonald, J. Mitchell, Cem. Concr. Res. 37 (2007) 295-302.

[19] P.J. McDonald, V. Rodin, A. Valori, Cem. Concr. Res. 40 (2010) 1656-1663.

[20] Y.Q. Song, Cem. Concr. Res. 37 (2007) 325-328.

[21] A. Valori, P.J. McDonald, K.L. Scrivener, Cem. Concr. Res. 49 (2013) 65-81.

[22] J.-P. Korb, Magn. Reson. Imaging 25 (2007) 466-469.

[23] R. Valckenborg, L. Pel, K. Kopinga, Magn. Reson. Imaging 19 (2001) 489-491.

[24] J.B.W. Webber, P. Corbett, K.T. Semple, O. Ogbonnaya, W.S. Teel, C.A. Masiello, Q.J. Fisher, J.J. Valenza, Y.Q. Song, Q. Hu, Microporous Mesoporous Mater. 178 (2013) 94-98.

[25] J.E. Birdwell, K.E. Washburn, Energy Fuels 29 (2015) 2234-2243.

[26] E. Rylander, P.M. Singer, T. Jiang, R.M. Schlumberger, S.S. Matador, SPE (2013) 164554.

[27] W. Schänfelder; J. Dietrich; A. Märten; K. Kopinga; F. Stallmach, Cem. Concr. Res. 37 (2007) 902-908.

[28] M. Fleury, E. Kohler, F. Norrant, S. Gautier, J. M'Hamdi, J. Barré, J. Phys. Chem. C117 (2013) 4551-4560.

[29] S. Godefroy, J.-P. Korb, M. Fleury, R.G. Bryant, Phys. Rev. E 64 (2001) 021605.

[30] G. Gannaway, SPE (2014) 173474-STU.

[31] R. Kausik, K. Fellah, E. Rylander, P.M. Singer, R.E. Lewis, S.M. Sinelair, NMR Relaxometry in shale and implications for logging, SPWLA 56th Annual Logging Symposium (2015) SPWLA-2015-SSS.

[32] K.E. Washburn, J.E. Birdwell, J. Magn. Reson. 233 (2013) 17-28.

[33] K.E. Washburn, Concepts Magn. Reson. A43 (2014) 57-78.

[34] P.J. Prado, B.J. Balcom, S.D. Beyea, T.W. Bremner, R.L. Armstrong, R. Pishe, P.E. Gratten-Bellew, J. Phys. D 31 (1998) 2040-2050.

[35] P. Pipilikaki, M. Beazi-Katsioti, Constr. Build. Mater. 23 (2009) 1966–1970.

[36] B. Zhou, Q. Han, P.-Q. Yang, Energy & Fuels 30 (2016) 9122-9131.

[37] K. Bartik, P. Choquet, A. Constantinesco, G. Duhamel, J. Fraissard, J.N. Hyacinthe, J. Jokisaari, E. Locci, T.J. Lowery, M. Luhmer, T. Meersmann, I.L. Moudrakovski, G.E. Pavlovskaya, K.L. Pierce, A. Pines, J.A. Ripmeester, V.-V. Telkki, W.S. Veeman, Actual. Chim. 287 (2005) 16-34.

[38] B.M. Goodson, J. Magn. Reson. 155 (2002), 157-216.

[39] D.A. Barskiy, A.M. Coffey, P. Nikolaou, D.M. Mikhaylov, B.M. Goodson, R.T. Branca, G.J. Lu, M.G. Shapiro, V.-V. Telkki, V.-V. Zhivonitko, I.V. Koptyug, O.G. Salnikov, K.V. Kovtunov, V.I. Bukhtiyarov, M.S. Rosen, M.J. Barlow, S. Safavi, I.P. Hall, L. Schröder, E.Y. Chekmenev, Chem. Eur. J. (23) 2017 725-751.

[40] M.S. Albert, G.D. Cates, B. Driehuys, W. Happer, B. Saam, C.S. Springer Jr., A. Wishnia, Nature 370 (1994) 199-201.

[41] J.P. Mugler 3rd, T.A. Altes, I.C. Ruset, I.M. Dregely, J.F. Mata, G.W. Miller, S. Ketel, J. Ketel, F.W. Hersman, K. Ruppert, Proc. Natl. Acad. Sci. U.S.A. 107 (2010) 21707-21712.

[42] C. Hilty, E.E. McDonnell, J. Granwehr, K.L. Pierce, S. Han, A. Pines, Proc. Natl. Acad. Sci. U.S.A. 102 (2005) 14960-14963.

[43] V.-V. Telkki, C. Hilty, S. Garcia, E. Harel, A. Pines, J. Phys. Chem. B 111 (2007) 13929-13936.

[44] J. Jokisaari, NMR of Noble Gases Dissolved in Liquid Crystals, In NMR of Ordered Liquids, E.E. Burnell, C.A. de Lange, Eds, Kluwer: Dordrecht (2003) 109.

[45] J. P. Jokisaari, A.M. Kantola, J.A. Lounila, L.P. Ingman, Phys. Rev. Lett. 106 (2011) 017801-1-017801-4.

[46] J.B. Miller, J.H. Walton, C.M. Roland, Macromolecules 26 (1993) 5602-5610.

[47] S. Glöggler, M. Raue, J. Colell, P. Türschmann, A. Liebisch, T. Mang, B. Blümich, S. Appelt, Chem. Phys. Chem. 13 (2012) 4120-4123.

[48] J. Roukala, J. Zhu, C. Giri, K. Rissanen, P. Lantto, V.-V. Telkki, J. Am. Chem. Soc. 137 (2015) 2464-2467.

[49] L. Schröder, Phys. Med. 29 (2013) 3-16.

[50] E. Weiland, M.-A. Springuel-Huet, A. Nossov, A. Gédéon, Microporous Mesoporous Mater. 225 (2016) 41-65.

[51] J. Demarquay, J. Fraissard, Chem. Phys. Lett. 136 (1987) 314-318.

[52] V.V. Terskikh, I.L. Moudrakovski, H.-B. Du, C.I. Ratcliffe, J.A. Ripmeester, J. Am. Chem. Soc. 123 (2001) 10399-10400.

[53] V.V. Terskikh, I.L. Mudrakovskii, V.M. Mastikhin, J. Chem. Soc. Faraday Trans. 89 (1993) 4239-4243

[54] V.V. Terskikh, I.L. Moudrakovski, S.R. Breeze, S. Lang, C.I. Ratcliffe, J.A. Ripmeester, A. Sayari, Langmuir 18 (2002) 5653-5656.

[55] E. Weiland, M.-A. Springuel-Huet, A. Nossov, F. Guenneau, A.-A Quoineaud, A.-A. Gédéon, J. Phys. Chem. C 119 (2015) 15285-15291.

[56] C. Tsiao, R.E. Botto, Energy & Fuels 5 (1991) 87-92.

[57] V.-V. Telkki, J. Lounila, J. Jokisaari, J. Phys. Chem. B109 (2005) 757-763.

[58] V.-V. Telkki, J. Lounila, J. Jokisaari, J. Phys. Chem. B109 (2005) 24343-24351.

[59]V.-V. Telkki, J. Lounila, J. Jokisaari, J. Chem. Phys. 124 (2006) 034711-134711-8.

[60] V.-V. Telkki, J. Lounila, J. Jokisaari, Phys. Chem. Chem. Phys. 8 (2006) 2072-2076.

[61] V.-V. Telkki, J. Lounila, J. Jokisaari, Magn. Reson. Imaging 25 (2007) 457-460.

[62] S.V. Filimonova, H. Knicker, W. Häusler, I. Kögel-Knabner, Geoderma 122 (2004) 25-42.

[63] C.D. Keenan, M.M. Herling, R. Siegel, N. Petzold, C.R. Bowers, E.A. Rössler, J. Breu, J. Senker, Langmuir 29 (2013) 643-652.

[64] M. Mauri, R. Simonutti, Materials 5 (2012) 1722-1739.

[65] P. Ngokoli-Kekele, M.-A Springuel-Huet, P.P. Man, J. Thoret, J. Fraissard, D.R. Corbin, Microporous Mesoporous Mater. 25 (1998) 35-41.

[66] J. Jeener, B.H. Meier, P. Bachmann, R.R. Ernst, J. Chem. Phys. 71(1979) 4546-4553.

[67] O.K. Kuvandikov, K.O. Shakarov, Z.M. Shodiev, G.R. Rabbimova, J. Commun. Tech. Electron. 52 (2007) 1062-1064.

[68] M. Hanni, P. Lantto, J. Vaara, Phys. Chem. Chem. Phys. 11 (2009) 2485-2496.

[69] I. Bertini, C. Luchinat, G. Parigi, Solution NMR of paramagnetic molecules. Elsevier, Amsterdam, 2001.

[70] L. Benda, J. Mareš, E. Ravera, G. Parigi, C. Luchinat, M. Kaupp, J. Vaara, Angew. Chem. Int. Ed. 55 (2016) 14713-14717.

[71] J. Vaara, S.A. Rouf, J. Mareš, J. Chem. Theory Comput. 11 (2015) 4840-4849.